Interaction between two large particles in a dry granular shear flow

Nathalie Fraysse, Umberto d'Ortona, Nathalie Thomas

Interaction between two large particles in a dry granular shear flow

Nathalie Fraysse
Université Côte d'Azur, CNRS, INPHYNI, Nice, France[*]

Umberto D'Ortona
Aix-Marseille Univ., CNRS, Centrale Marseille, M2P2, Marseille, France[†]

Nathalie Thomas
Aix-Marseille Univ., CNRS, IUSTI, Marseille, France[‡]

(Dated: November 28, 2022)

The interaction between two large particles (called tracers) in a dry granular flow made of small particles is studied experimentally and numerically. Depending on the size ratio between tracers and small particles (ranging from 6 to 13) and on the flow thickness (ranging from 6 to 30 small particle diameters) three different regimes are observed. For thin flow thicknesses, tracers get close while flowing and remain in contact. For intermediate thicknesses, tracers flow at a defined distance that increases with the flow thickness, and for large thicknesses, there is an abrupt transition above which tracers move away from each other. The transitional flow thickness increases with tracer size. More surprisingly, for all tracer sizes and all flow thicknesses, tracers get aligned with the flow. These features are explained through a mechanism involving the path of the front tracer which favors tracers regrouping, and the velocity gradient of the flow which tends to repel the tracers. Both are linked through the vertical and longitudinal spacings between tracers which modulate these effects.

I. INTRODUCTION

The numerous occurrences in natural and industrial environments of flows of polydisperse dry granular materials have attracted much attention and driven many experimental, numerical and theoretical studies for a long time [1–3]. Most of these studies deal with mixtures of two sizes of particles of the same density, small size ratios between the large and small particles (smaller than 4, typically) and more or less the same fractions of both species. These conditions lead to the usual granular size segregation pattern, with large particles moving toward the free surface of the flow [4–6]. Notwithstanding, it was shown that the opposite takes place for high size ratios and low fractions of large particles, still of the same density as the small particles. The large and, consequently, heavy particles can then push away the small ones and make their way down the flowing granular layer. For instance, a few large particles in a shear flow down a rough incline migrate downward and stabilize near the bottom of the flow for size ratios larger than about 4.5. This phenomenon was called reverse segregation [7–9]. It can be thought of in terms of buoyancy: as the flowing small particles have a volume fraction around 0.6, the density ratio between a large particle and the equivalent volume of the surrounding small particles having the same intrinsic density tends to 1.7 for very large particles.

Several investigations of the forces acting on objects immersed in a granular flow have been performed, most of them considering one or more static intruders to study the drag forces on these obstacles to the flow [10, 11] The dynamics of an intruder free to move in the granular flow has been addressed only marginally [12]. To our knowledge, the interaction between large particles has never been studied, even though it is likely to be of great relevance in debris flows and industrial processes.

This situation strongly contrasts with that of particles suspended in fluids. Among other issues, the interaction between sedimenting particles has been studied for long [13–22]. The dynamics of solid spheres settling in a Newtonian fluid has proved to exhibit a rich phenomenology including the Drafting-Kissing-Tumbling behavior [23–25] and may result in peculiar patterns [26–28] in the arrangement of the particles. In sheared suspensions, different migration behaviors are observed depending on the flow conditions and the properties of the particles and of the fluid. Particles may attract or repel each others, which leads to microstructures like trains of particles in channel flows [29, 30]. In the case of non-Newtonian fluids, even more complex phenomena may arise, like repulsion between particles for a shear-thickening fluid, or alignment in viscoelastic fluids [31].

In a somewhat similar approach, this work focuses on the dynamics of two large particles in a dry granular shear flow made of small particles, in situation of reverse segregation. All particles have the same intrinsic density. Two investigation methods, experimental and numerical, have been implemented. Regarding simulations, the Distinct Element Method (DEM) [32] was used. Its performance makes possible a thorough study of various parameters and gives access to quantities that would be difficult, if not impossible, to measure experimentally. Conversely, experiments provide the necessary validation of the simulation results.

In this article, we present a study of the interaction

* nathalie.fraysse@univ-nice.fr
† umberto.dortona@cnrs.fr
‡ nathalie.thomas@univ-amu.fr

between two large particles, called tracers hereafter, in a granular flow down a rough incline. The article is organized as follows. The experimental protocol and the numerical scheme are described in Section II. Section III introduces the physical phenomenon, from both experiments and simulations. Section IV reports a parametric numerical study of the influence of the tracer size, the thickness of the granular flow, the slope of the incline and its roughness. A mechanism for the interaction process is proposed and discussed in part V. Section VI ends the article with conclusions

II. METHODS

A. Experimental protocol

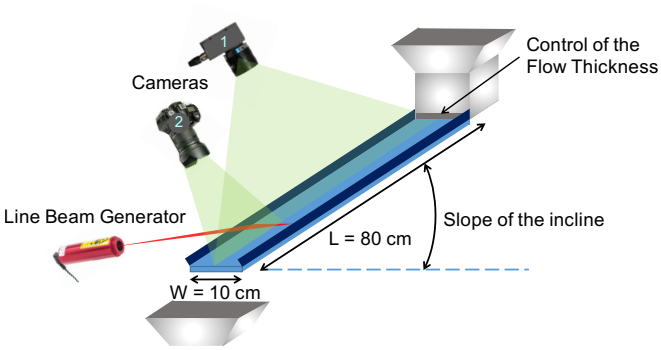

FIG. 1. Sketch of the experimental set up.

Experiments have been conducted on a 80 cm long and 10 cm wide incline (Fig. 1). The incline is made rough by covering the board with a grade P120 sandpaper. Its slope is set to 23°. Flowing particles are glass beads (density $\rho = 2500$ kg m^{-3}) that have been sieved between 300 μm and 400 μm, with a size distribution centered close to $d = 350$ μm. Tracers are coloured glass beads (density $\rho = 2580$ kg m^{-3}) of same diameter d_t, equal to either 2.0 mm or 3.5 mm, which leads to two size ratios d_t/d of about 6 and 10. A feeding container of an approximate volume of two liters is placed at the top of the incline. The flow rate from the hopper and thus the thickness of the granular flow are controlled by the height of the container gate. Its width is kept constant, equal to the channel width. Ambient humidity is kept around 50%RH. After the opening of the container gate, a steady, uniform flow of small glass beads establishes over the entire channel. Soon after, 2 tracers are gently dropped on the flow, about 10 cm below the gate as the flow thickness might not be constant close to the exit. A homemade injector is used to approximately set the initial relative location of the tracers. The tracers are driven downwards; they rapidly reach their stationary height inside the granular flow, after a few centimeters of travel. A high-resolution video camera with a wide-angle lens, placed above the channel, images its entire length while a digital still camera zooms in on its lower part. The positions of the tracers are obtained from videos recorded at 25 fps typically as well as from photos captured in burst mode. The thickness of the granular flow is measured from the shift of the shadow of a thin tense string or from the deflection of a laser sheet. Flow thickness from 2.2 mm to 3.0 mm have been studied experimentally.

B. Numerical model

The numerical method used is the distinct element method (DEM). A linear-spring and viscous damper force model [32, 33] is implemented to calculate the normal force between contacting particles. The details on the numerical model and its parameters (normal stiffness, normal damping, collision time and restitution coefficient) have been published previously and can be found in [9, 33, 34]. The gravitational acceleration is $g = 9.81\,\mathrm{m\,s^{-2}}$. The particle properties correspond to those of cellulose acetate: density $\rho = 1308\,\mathrm{kg\,m^{-3}}$, restitution coefficient $e = 0.87$ and friction coefficient $\mu = 0.7$ [33, 35]. To prevent the formation of a close-packed structure, the small particles have a uniform size distribution ranging from $0.95d$ to $1.05d$, with d hereafter referred to as the small-particle diameter. d is equal to 6 mm in the simulations. The large particle diameter is d_t. The collision time is $\Delta t = 10^{-4}$ s, consistent with previous simulations [35–37] and sufficient for modeling hard spheres [38, 40, 41]. These parameters correspond to a stiffness coefficient $k_n = 7.32 \times 10^4$ N m^{-1} [33] and a damping coefficient $\gamma_n = 0.206$ kg s^{-1}. The integration time step is $\Delta t/50 = 2 \times 10^{-6}$ s to meet the requirement of numerical stability [38].

The initial configuration is obtained as follows. Small beads are placed randomly in the simulation domain, along with two large particles that are placed at $0.75d_t$ above the bottom, aligned or not, close or away depending on the simulation. During 0.3 s, gravity is set perpendicular to the bottom plane and particles fall. All beads touching the bottom of the domain stop moving and form a monolayer of bonded particles which generates the roughness of the incline. The other beads will constitute the flowing granular material. This procedure yields rough planes whose compacity is around 0.57. The particles of the rough bottom have the same size as the small flowing particles, except for one particular study on the effect of the roughness of the incline, where various diameters of particles, from $d_i = 0.9d$ to $1.5d$, were used to generate the glued monolayer (see Sec. IV E). After 0.3 s, gravity is tilted to the chosen slope (24°, except in Sec. IV D) and the flow starts. Rough-bottom particles are assumed to have an infinite mass for calculation of the collision force between flowing and fixed particles. The velocity-Verlet algorithm is used to update the position, orientation, and linear and angular momenta of each particle. Periodic boundary conditions are applied in the flow direction x and in the transverse direction y of the

simulation domain. The size of the domain is $L_x = 80d$ and $L_y = 40d$ in the x and y directions, except in some cases for which the size is increased up to $160d \times 80d$. The positions and velocities of all particles, including the tracers, are stored every 0.1 s for post-processing purpose. The thickness of the moving granular layer is computed from the surface ($z = 0$) of the roughness of the incline, one small-particle diameter higher than the domain bottom. In part V, virtual springs are added between tracers in order to maintain them at a defined distance (in the plane of the incline) or to constrain their height difference (perpendicular to the plane of the incline).

III. RESULTS: EVIDENCE OF AN INTERACTION BETWEEN TRACERS

A. First observations

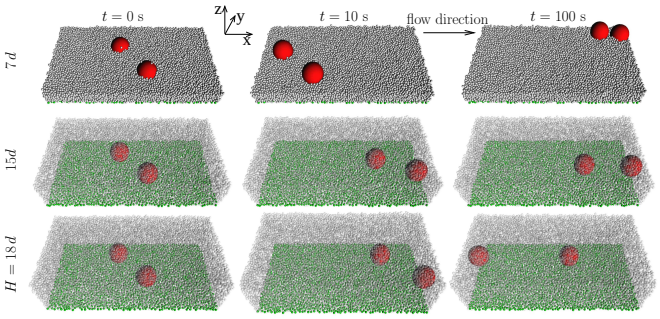

FIG. 2. From the numerical simulations, three successive positions of 2 tracers (in red) in dry granular flows of small particles (in grey). Particles of the rough incline are green. The size ratio between the large and small particles is $d_t/d = 10$. Three thicknesses of the flow are displayed: $H = 7d$, $15d$ and $18d$. The simulation domain is $80d \times 40d$ and the slope of the incline is 24°. Also see videos 1 to 3 in Supplemental Material [39].

In the first part of the numerical study, the size ratio of the tracer diameter to the small-particle diameter is set to $d_t/d = 10$. This size ratio ensures reverse segregation [7, 9]. Three flow thicknesses were implemented ($H = 7d$, $15d$ and $18d$). In the initial configuration ($t = 0$ s), the two tracers are aligned at 45° of the flow direction and the distance between their centers is twice the tracer diameter, as illustrated in the left column of Fig. 2. The equilibrium position of the tracers in the z-direction, near the bottom of the granular flow, results from the reverse segregation mechanism and the difficulty to penetrate the lowest small-particle layers where chain forces are efficient enough to support a large particle. For the thinnest flow, tracers are large enough to emerge from the flow and are visible at its surface. For the two thick flows, tracers are completely embedded in the granular flow and small particles are drawn partly transparent in Fig. 2 to make the tracers visible.

The simulations bring to light a striking behavior of the tracers in the granular flow. For the thin flow case ($H = 7d$), they are observed to align in the flowing direction and eventually get in contact. Tracers attract each other. For the two thick flow cases, the tracers also align but move away from each other, to a distance depending on the flow thickness. For $H = 15d$, tracers locate at a distance (measured from center to center) $\Delta x \simeq 20d$. For $H = 18d$, this distance is $\Delta x \simeq 37d$, which is close to the maximal distance ($\Delta x = 40d$) which can be obtained for periodic boundary conditions and a simulation domain length of $L = 80d$. An increase in the simulation domain length shows that tracers actually repel each other for the thickest flow (see below).

It is interesting to note that when tracers are close and not perfectly aligned, they migrate in the transverse direction (perpendicular to the flow) and towards the front tracer. This is not visible in Fig. 2 due to the periodic boundary conditions but visible in video 1, corresponding to $H = 7d$. When the flow is thick, and tracers are far away, no migration is visible (see video 2 and 3). Such a behaviour is also observed for particles sedimenting in a fluid. The study of the this phenomenon is ongoing and will be presented in a future work.

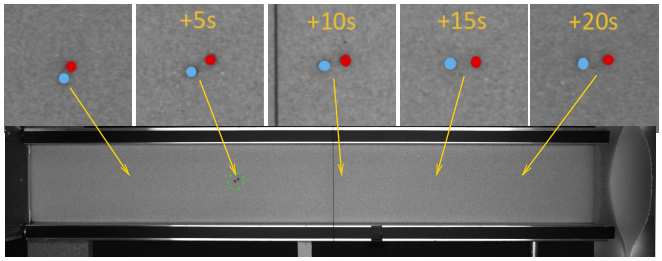

FIG. 3. Pictures from an experiment performed with a granular flow made of small particles of diameter $d \simeq 350$ μm and two large tracers of diameter $d_t = 2.0$ mm, for a size ratio $d_t/d \simeq 6$. The slope of the incline is 23°. The flow thickness is $H = 2.2$ mm $\simeq 6.5d$. The lower picture shows the whole plane, with one location of the tracers highlighted by a green dashed circle as an example. The five upper sub-images illustrate the time evolution of the relative position of tracers; the arrows indicate their corresponding locations on the plane.

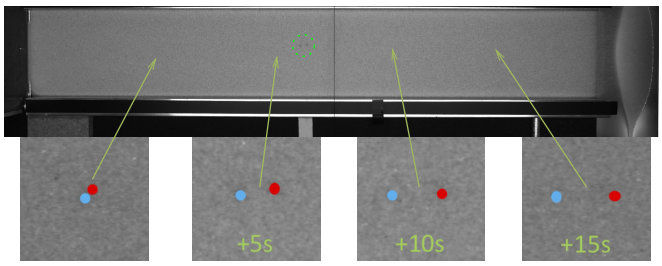

FIG. 4. Same as Fig. 3 for a larger granular flow thickness $H = 2.9$ mm $\simeq 8.5d$. The four lower sub-images show the time evolution of the relative position of the tracers.

A similar qualitative behavior is observed experimentally. Figures 3 and 4 show two experiments performed for the same size ratio ($d_t/d \simeq 6$) and two flow thicknesses. The small beads have a diameter $d \simeq 350\,\mu$m and the tracer diameter is 2.0 mm. The flow thicknesses are $H = 2.2\,$mm $\simeq 6.5d$ and $H = 2.9\,$mm $\simeq 8.5d$ for Figs. 3 and 4, respectively. Note that the particles flow toward the right in these figures. The sub-images display the time evolution of the tracer positions. To facilitate the visualization, their locations are highlighted by two red and blue circles which have the same diameter as the tracers and stand for the front and back tracers, respectively.

Like in simulations, for both flow thicknesses, the two tracers get aligned with the flowing direction. Tracers, which are initially in contact, move away while flowing. For the thinnest flow (Fig. 3), the tracers eventually locate at a distance $\Delta x \simeq 2.5 d_t \simeq 15d$ from center to center. For the thickest flow (Fig. 4), the distance between the tracer centers continuously increases until tracers reach the end of the incline, where the distance comes to $\Delta x \simeq 30d$.

Experiments performed with tracers 3.5 mm in diameter, i.e. a size ratio $d_t/d \simeq 10$, and two flow thicknesses $H \simeq 2.6$ mm $\simeq 7.5d$ and $H \simeq 3.0$ mm $\simeq 9d$, all else being equal, show that tracers also align but they stay, or rapidly come in contact.

Thus, numerical simulations and experiments demonstrate that two large particles in a dry granular flow down an incline do interact. Both approaches suggest that two regimes exist, attractive or repulsive depending on the thickness of the flow.

B. Time evolution of the relative position of the tracers

The time evolution of the relative position of the two tracers give further details on the process. Figures 5, 6 and 7 report the longitudinal (Δx, upper curves) and transverse (Δy, lower curves) distances between the tracer centers as a function of time, for the numerical and experimental studies reported above.

As exemplified in Fig. 5, the numerical simulations performed for a size ratio $d_t/d = 10$ show that a stationary regime is reached after a transition period whose duration increases with the flow thickness. The transverse distance (Δy) converges toward zero for all values of the flow thickness, rapidly for a thin flow and more slowly for a thicker flow. Whereas the longitudinal distance (Δx) also converges to a steady state, it exhibits various behaviors of which Fig. 5 gives a representative example. For the thinner flow ($H = 7d$), the longitudinal distance tends to d_t, showing that tracers are almost in contact. For $H = 15d$, the longitudinal distance fluctuates around $\Delta x = 20d$. For the thickest flow ($H = 18d$), the longitudinal distance reaches almost $\Delta y = 40d$, which corresponds to half of the simulation domain length. Due

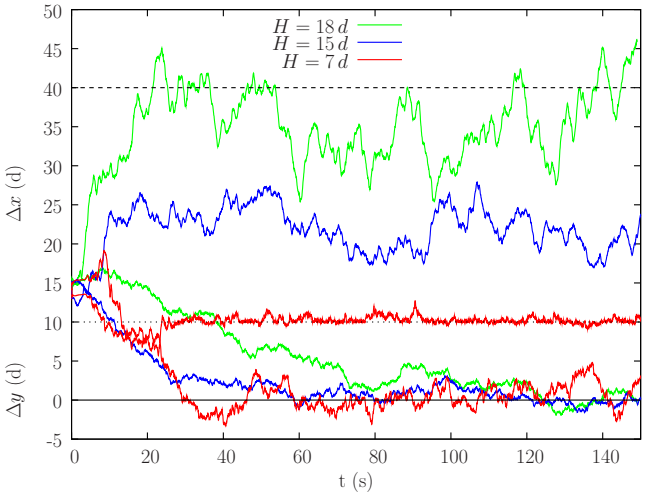

FIG. 5. Longitudinal (Δx, upper curves) and transverse (Δy, lower curves) distances between the two tracer centers ($d_t/d = 10$) measured in small bead diameter (d), as a function of time, for the three flow thicknesses ($H = 7d$, $15d$ and $18d$) of the numerical study corresponding to Fig. 2. The transverse distances Δy converge to zero. The longitudinal distances tend to different values increasing with the flow thickness. The dotted line indicates one tracer diameter $d_t = 10d$, i.e. the minimal longitudinal distance between two tracer centers perfectly aligned with the flow direction. The dashed line ($y = 40d$) corresponds to half of the longitudinal size of the simulation domain, i.e. the maximum distance that two aligned repelling tracers can reach.

to the periodic boundary conditions used in the simulations, this is the maximum distance that can be reached between two repelling tracers since they interact by both sides of the simulation domain.

Figures 6 and 7 show the time evolution of the longitudinal (Δx, upper curves) and transverse (Δy, lower curves) distances between the two tracer centers in the experiments performed for two size ratios. In Fig. 6, for the size ratio $d_t/d \simeq 10$ and the two small flow thicknesses investigated, the behaviors observed are the same as in the simulations for the thinnest flow. Tracers align and come in contact. In Fig. 7, for the size ratio $d_t/d \simeq 6$ and a thin flow ($H \simeq 6.5d$, blue curves), the transverse distance Δy also decreases and tends to zero, i.e. tracers get aligned, whereas the longitudinal distance Δx rapidly growths to $10d$, and then reaches some kind of plateau around $15d$, followed by a slight increase which could be due to a non-constant flow thickness. For the same size ratio $d_t/d \simeq 6$ and a thick flow ($H \simeq 8.5d$, red curves in Fig. 7), the transverse distance Δy also decreases, more slowly than for the thin flow, and does not reach zero before the end of the incline. The longitudinal distance Δx rapidly reaches a value around $\Delta x \simeq 30d$ and fluctuates around it. Note that the curves for the thick case end more rapidly than for the thin case since the flowing velocity increases with the flow thickness. Repeated measurements at a given size ratio and flow thickness show

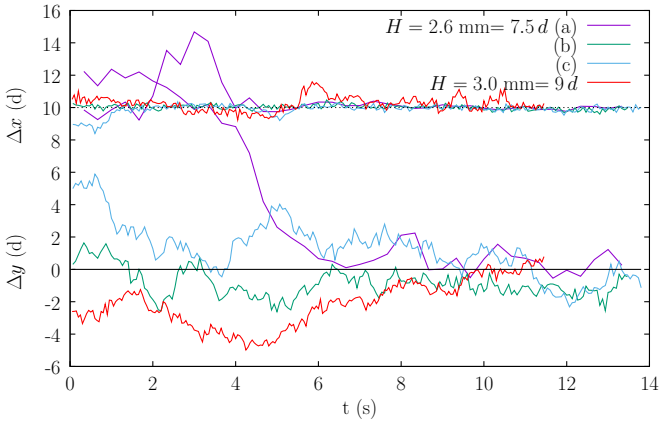

FIG. 6. Longitudinal (Δx, upper curves) and transverse (Δy, lower curves) distances between the two tracer centers measured in small bead diameter (d) for four experiments performed for a size ratio $d_t/d \simeq 10$ and two flow thicknesses $H = 2.6$ mm $\simeq 7.5d$ and $H = 3.0$ mm $\simeq 9d$. The dotted line indicates one tracer diameter $d_t = 10d$, i.e. the minimal longitudinal distance between two tracer centers perfectly aligned with the flow direction.

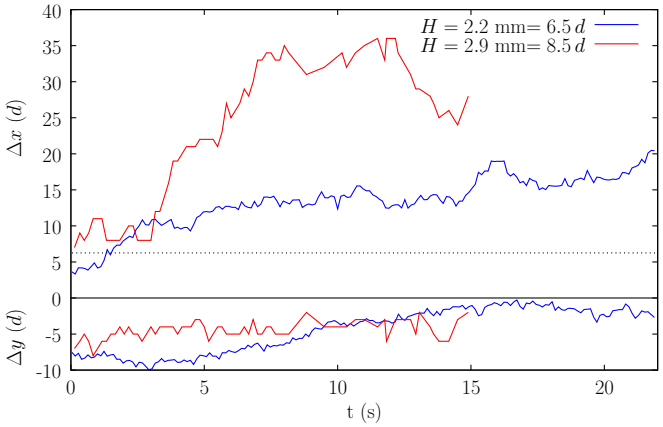

FIG. 7. Longitudinal (Δx, upper curves) and transverse (Δy, lower curves) distances between the two tracer centers measured in small bead diameter (d) for the two experiments corresponding to Figs. 3 and 4, respectively. The size ratio is $d_t/d \simeq 6$ and the flow thicknesses are $H = 2.2$ mm $\simeq 6.5d$ and 2.9 mm $\simeq 8.5d$. The dotted line indicates one tracer diameter $d_t = 6d$, i.e. the minimal longitudinal distance between two tracer centers perfectly aligned with the flow direction.

that tracers eventually locate at similar relative positions.

Fluctuations in Fig. 5 draw attention. Regarding the longitudinal distance Δx between tracers, fluctuations grow at increasing flow thickness, from almost null when tracers have come in contact at small flow thickness, to large when tracers are far away from one another at large flow thickness. Likewise, in the experiments reported in Figs. 6 and 7, fluctuations on Δx are larger when tracers are far apart than for tracers in contact. Logically, the further the tracers, the weaker the interaction between them and the less their relative position is constrained.

Regarding the transverse distance Δy, the amplitude of its fluctuations is rather small in the steady state. Fluctuations on Δy do not show a clear correlation with the thickness of the flow nor with the longitudinal distance.

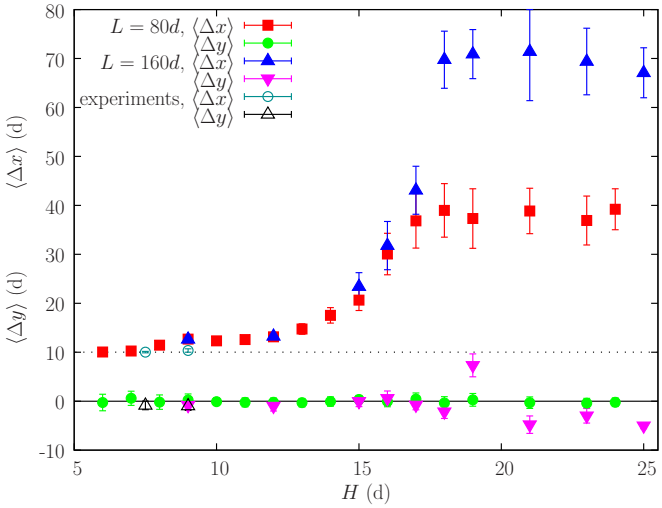

FIG. 8. Mean longitudinal $\langle \Delta x \rangle$ and transverse $\langle \Delta y \rangle$ distances (measured from center to center and stated in small-particle diameter d) between two tracers of size ratio $d_t/d = 10$ at increasing flow thicknesses. In simulation (filled symbols), the domain size is $80d \times 40d$ (red squares and green circles) or $160d \times 40d$ (blue triangles and purple reverted triangles). The empty symbols (cyan circles and black triangles) stand for the experiments performed at a size ratio $d_t/d \simeq 10$. The dotted line indicates one tracer diameter $d_t = 10d$, i.e. the minimal longitudinal distance between two aligned tracers.

C. Numerical study of the steady state

Figures 5 to 7 confirm the existence of a transition between two regimes of interaction between the tracers, attractive at small flow thickness and repulsive at large flow thickness. This transition can be highlighted by considering the average values computed on the steady state in the numerical simulations.

Figure 8 plots the mean longitudinal $\langle \Delta x \rangle$ and transverse distances $\langle \Delta y \rangle$ obtained numerically between the tracer centers, as a function of the flow thickness in the range $H = 6d$ to $25d$, for the size ratio $d_t/d = 10$. The error bars indicate the standard deviation of the distances. To compute the mean, the first 50 s of each simulation are discarded to ensure that the stationary regime has been reached. In a few cases, tracers were not aligned after 50 s and the averaging was started only when tracers got aligned. Averaging is typically performed for a period of 200 s. To probe the effect of periodic boundary conditions, two domain sizes were considered: the size previously used, $80d \times 40d$, was increased to $160d \times 40d$, for a few cases only since simulations become numerically costly for such a large domain.

For all flow thicknesses and both domain sizes, the mean transverse distance $\langle \Delta y \rangle$ is close to zero, which confirms that tracers always tend to align with the flow direction. The mean longitudinal distance $\langle \Delta x \rangle$ shows a transition around $H = 17d$. Below this thickness, for both domain sizes, tracers locate at a defined distance that decreases at decreasing flow thickness. This decrease is limited by the size of the tracers since, once aligned, the longitudinal distance between tracers cannot be smaller than one tracer diameter, which corresponds to tracers in contact. In this range of flow thickness smaller than $17d$, the standard deviations are very small, indicating that the attraction between tracers is strong enough not to be sensitive to the fluctuations inherent to a granular flow. Note that the experimental behavior reported in Fig. 6 for a size ratio $d_t/d \simeq 10$ and small flow thickness (empty symbols in Fig. 8) is consistent with the numerical results. In contrast, for large flow thicknesses, the mean longitudinal distance reaches the maximum possible distance considering periodic boundary conditions, i.e. $\langle \Delta x \rangle \simeq 40d$ or $80d$ according to the domain size. Standard deviations are large since longitudinal distances strongly fluctuate in this repulsive regime, as emphasized above. Regarding the influence of the simulation domain size, it is interesting to note that, for flow thickness $H \geq 18d$, the tracers align with the flow in a less efficent way for the long than for the small simulation domain. The mean transverse distance $\langle \Delta y \rangle$ reaches value as large as $7d$.

Figure 8 makes the transition between an attractive and a repulsive regime clear for the size ratio $d_t/d = 10$. To gain a better knowledge on this transition, the size ratio between the tracers and the small particles, the slope of the incline and its roughness were varied in the numerical simulations. As before, the mean longitudinal and transverse distances are measured for various flow thicknesses. In addition, the vertical locations of the tracers within the granular flow are investigated.

IV. PARAMETRIC STUDY

A. Shift of the transition toward increasing flow thicknesses at increasing size ratio

Three additional size ratios are studied numerically, namely $d_t/d = 6$, 8 and 12. Below a size ratio of 6, tracers undergo a classical surface segregation and are no longer near the bottom of the flow. For size ratios larger than 12, the transition occurs for very large flow thicknesses and the computational cost strongly increases.

Figure 9 reports the mean transverse and longitudinal distances as a function of the flow thickness. All tracer sizes lead to the same overall shapes for these curves, however, the repulsive regime is reached at larger flow thickness for larger tracers, around $11d$, $13d$, $18d$ and $22d$ for tracers of diameters $d_t = 6d$, $8d$, $10d$ and $12d$, respectively. The transition between the attractive and repulsive regimes proves to depend on the tracer size.

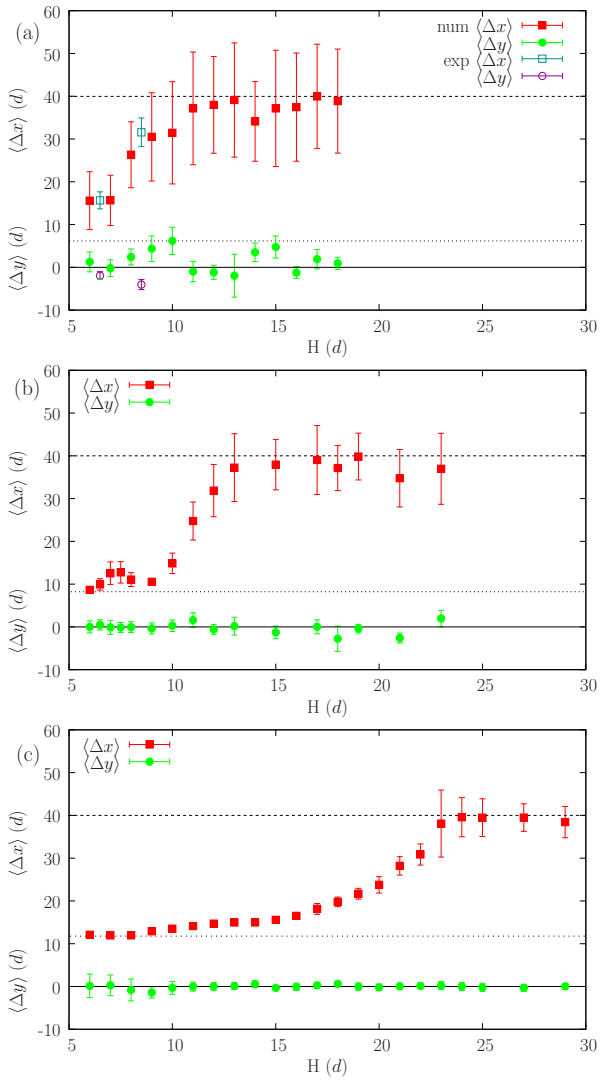

FIG. 9. Mean longitudinal $\langle \Delta x \rangle$ and transverse $\langle \Delta y \rangle$ distances between two tracers at increasing flow thicknesses. The size ratios between tracers and small particles are (a) $d_t/d = 6$, (b) $d_t/d = 8$ and (c) $d_t/d = 12$. The range in flow thickness, starting at $H = 6d$, is adjusted to reach the repulsive regime. The axis scales are kept identical for all graphs to facilitate comparison. All lengths are given in units of small-particle diameter. The dotted lines indicate the tracer diameters. In Fig. 9 (a), the empty symbols stand for the experiments performed at $d_t/d \simeq 6$.

Some less important differences between the three graphs in Fig. 9 can be noted. In particular, for the lower size ratio $d_t/d = 6$ (Fig. 9(a)), the mean longitudinal distance always presents a large standard deviation, even for the lowest flow thicknesses, and the mean transverse distance more or less deviates from zero. In addition, the lower limit of the attractive regime, where tracers are in contact, is not reached at the smallest flow thickness $H = 6d$ reported. This would require to lower the thickness even further. However, this is not possible in the

simulations since a granular layer thinner than $6d$ does not flow. For the size ratio $d_t/d = 6$ and a flow thickness large enough for the flow to occur, the attraction between tracers is not strong enough for the tracers to come in contact, neither to fully align while flowing. The mean longitudinal and transverse distances obtained experimentally for the size ratio $d_t/d \simeq 6$ and for $H \simeq 6.5d$ and $H \simeq 8.5d$ (see Fig. 7) are reported in Fig. 9(a). The agreement with the mean longitudinal distances obtained in simulations, $\Delta x \simeq 16d$ for $H = 6d$ and $\Delta x \simeq 30d$ for $H = 9d$, is noticeable.

Tracers with size ratios $d_t/d = 8$ and 12 (Fig. 9(b-c)) present similar behavior compared to the case $d_t/d = 10$ (Fig. 8). For thin flows, the tracers attract each other and locate at a defined distance that depends on the flow thickness. For the lower flow thicknesses, the mean longitudinal distance $\langle \Delta x \rangle$ is close to one tracer diameter and tracers are in contact. Standard deviations are small in the attractive regime. For thick flows, tracers repel each other, the mean longitudinal distance $\langle \Delta x \rangle$ is close to $L_x \simeq 40d$ and fluctuations are large.

Similar attractive and repulsive regimes are found for all the size ratios that were explored numerically. Figure 10, where intermediate size ratios $d_t/d = 7$, 9, 11 and 13 are also reported, depicts the attractive-repulsive transition for all the size ratios investigated. Note that the points above the transition have been omitted since the longitudinal distance in the repulsive regime is set by the numerical domain size, around $\Delta x = 40$, and has no physical meaning. The curves of the mean longitudinal distance versus flow thickness all present a similar shape, however the transition is seen to shift toward higher values of flow thickness and become smoother and smoother as the tracer size increases. For example, for the size ratio $d_t/d = 8$, an increase in flow thickness from $H = 9d$ to $H = 13d$ is enough to switch from tracers in contact to the repulsive regime, while for the size ratio $d_t/d = 12$, an increase in flow thickness from $H = 15d$ to $H = 23d$ is necessary. A practical consequence is that using large tracers makes it easier to differentiate the various regimes. However, this requires thick granular flows that are numerically expensive and complex to generate experimentally.

B. Vertical locations of the tracers

Numerical simulations also give access to the height of the tracers within the granular flow. Figure 11 plots the mean vertical locations of the two tracers above the rough incline ($z = 0$), for the size ratio $d_t/d = 10d$ and various flow thicknesses. Note that compared to previous graphs, the vertical axis is strongly stretched.

The main feature of Fig. 11 is that, whereas both tracers adopt an identical vertical position in the flow at flow thickness larger than 18 d, the front tracer stabilizes higher than the back tracer when the flow thickness becomes smaller than 18 d. Figure 8 shows that the value

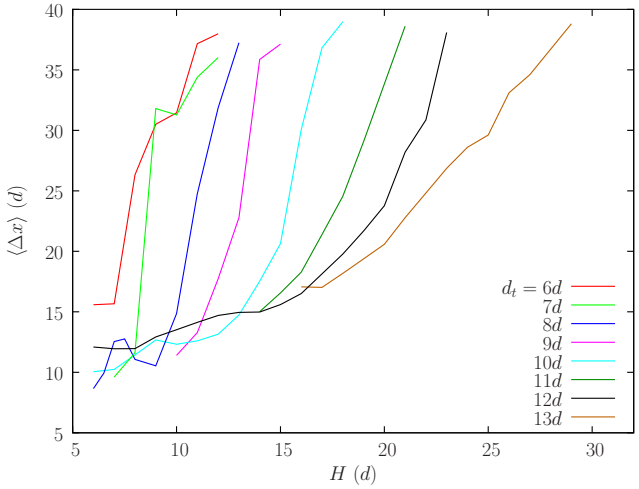

FIG. 10. Mean longitudinal distance $\langle \Delta x \rangle$ versus flow thickness for tracer sizes ranging from $d_t/d = 6$ to 13. All lengths are given in units of small-particle diameter d.

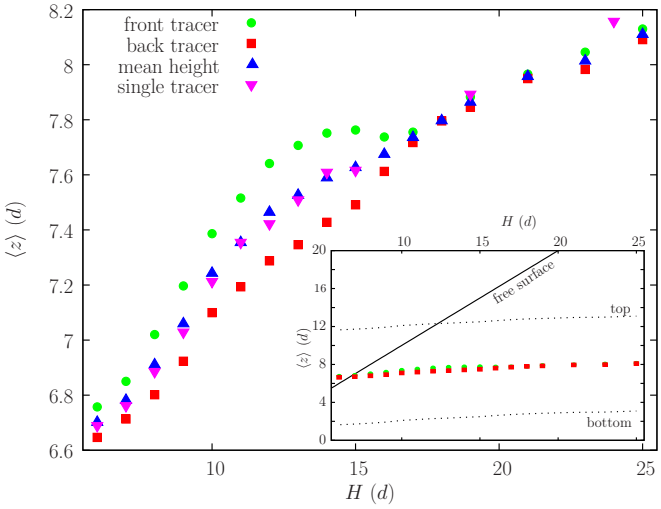

FIG. 11. Mean vertical positions of the front (green circles) and back (red squares) tracers ($d_t = 10d$) versus flow thickness H. The center of mass of the two tracers (blue triangle) as well as the vertical position of one single tracer in a similar flow (purple reverted triangle) are also plotted for comparison. All lengths are given in units of small-particle diameter. $z = 0$ corresponds to the surface of the rough incline, defined by the summit of the small glued particles (See II B)). The insert zooms out to visualize the vertical positions of the front-tracer top and bottom (dotted lines) compared to the free surface (solid line) of the granular flow.

$H = 18d$ corresponds to the transition between the two regimes of interaction for the size ratio $d_t/d = 10$. More specifically, the interaction between the tracers become purely repulsive above this value. Since tracers are far away from each other, they no longer alter the flow in the vicinity of the other tracer and their heights are identical. Below the value $H = 18d$, Fig. 11 shows that the mean height difference between the tracers $\langle \Delta z \rangle$ increases

when the flow thickness decreases down to $H = 13d$, then decreases again as the thickness further decreases from $H = 13d$ down to $H = 6d$ (also see Fig. 13). Since the tracers are closer and closer as the flow thickness decreases from $H = 18d$ (see Fig. 8), their interaction strengthens and a larger effect on their height difference $\langle \Delta z \rangle$ is expected. The following decrease in height difference when the flow thickness goes under $H = 13d$ results from the emergence of the tracers as exposed below. Figure 12 shows that the same phenomena occur for tracers of size $d_t/d = 12$ but for larger flow thicknesses. The tracers flow at the same height at large flow thickness, down to $H \simeq 23d$, which corresponds to the attractive-repulsive transition for this size ratio (from Fig. 9(c), also see Fig. 13). The mean height difference between tracers increases for flow thicknesses decreasing further, down to $H = 16d$, then starts to decrease.

The insets of Figs. 11 and 12 present the positions of the summit, center and bottom of the front tracer, as well as the location of the free surface of the flow. The mean vertical position of the back tracer is also reported to highlight that the height difference between the two tracers $\langle \Delta z \rangle$ is extremely small, less than half of a small particle diameter. The top dotted line intersects the free surface line for a flow thickness $H \simeq 13d$ for the tracer size $d_t/d = 10$ and $H \simeq 14.5d$ for $d_t/d = 12$. These values are close to those for which the height difference between the tracers starts to decrease. This shows that the decrease in the height difference occurs when the tracers get close to the free surface and eventually start to emerge from the granular flow, with a larger and larger emerged part when the flow thickness decreases further. Conversely, tracers are fully immersed for flows with larger thickness. As a consequence, for flow thicknesses smaller than $13d$ ($d_t/d = 10$) or $14.5d$ ($d_t/d = 12$), an extra buoyancy due to the emerging part of the tracers counterbalances the interaction between tracers and reduces the resulting height difference between them, more and more as the emerged part grows. This explains the decrease in height difference observed at decreasing thickness from about $H = 13d$ in Fig. 11 and $H = 16d$ in Fig. 12.

Figures 11 and 12 call for two more comments. The center of mass of the two tracers as well as the vertical position of one single tracer in a similar flow are also plotted. This shows that, for all flow thicknesses, the center of mass of the two tracers approximately coincides with the vertical location of one single tracer in simulations performed at the same flow thickness. This is expected at large flow thickness when tracers are far apart and flow at the same height, but this remains valid at small flow thickness when a height difference between the tracers is observed. Thus, the attractive interaction between the tracers causes a lift of the front tracer and a sink of the back tracer while their center of mass settles at a vertical position very close to that of a single tracer.

The second remark relates to the tracer height above the rough bottom. The bottom dotted line in the inset of Fig. 11 gives the position of the front-tracer bottom

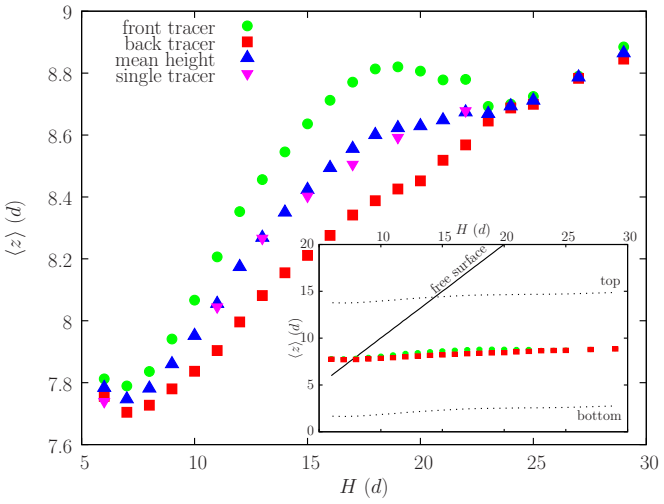

FIG. 12. Mean vertical positions of the front (green circles) and back (red squares) tracers ($d_t = 12d$), center of mass of the two tracers (blue triangle), and the vertical position of one single tracer in a similar flow (purple reverted triangle) versus flow thickness H. All lengths are given in units of small-particle diameter. $z = 0$ corresponds to the surface of the rough incline, defined by the summit of the small glued particles (See II B)). The inset zooms out to visualize the vertical positions of the front-tracer top and bottom (dotted lines) compared to the free surface (solid line) of the granular flow.

and shows that, even though tracers are in a reversed-segregated location, they do not touch the rough incline ($z = 0$). A layer of small particles, two to three small-particles diameter thick, flows under the tracer bottom. Its thickness slightly increases with the flow thickness. The same is observed for the tracer size $d_t/d = 12$ (Fig. 12).

C. A criterion to define the transition thickness

Figure 13 reports the mean height difference $\langle \Delta z \rangle$ between the front and back tracers as a function of the flow thickness, for all the tracer sizes that have been simulated, ranging from $d_t = 6d$ to $13d$. At decreasing flow thickness, all curves display an increase of $\langle \Delta z \rangle$ followed by a decrease when tracers are emerging. Accordingly, the maximum of the curve shifts towards low flow thicknesses for decreasing tracer sizes. For the case $d_t = 6d$, this decrease does not appear in Fig. 13 as it would start at a flow thickness that is too small for the flow to occur in the simulation.

The tracer height difference conveniently provides an unambiguous mean to define the transition between the attractive and the repulsive regimes. As illustrated in Fig. 13 for the size ratio $d_t/d = 11$, the intersection with the horizontal axis ($\langle \Delta z \rangle = 0$) of a second-order polynomial fit of the decreasing part of the curve gives a value of the flow thickness beyond which the interaction be-

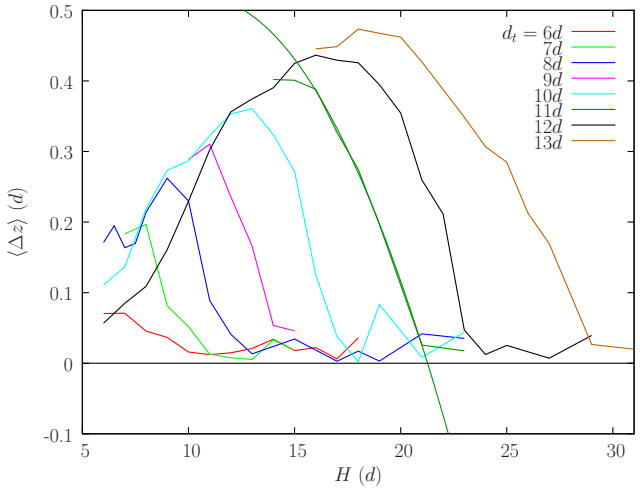

FIG. 13. Mean tracer height difference ($\langle \Delta z \rangle$) versus flow thickness H for tracer size ranging from $d_t = 6d$ to $13d$. For the size ratio $d_t/d = 11$, a second-order polynomial fitted on the descending part of the graph is shown. The intersection of this fit with the horizontal axis is used to define the transition thickness H^*. All lengths are given in units of small-particle diameter.

tween tracers is purely repulsive and both tracers have the same height. This value is called the transition thickness, noted H^*. For $d_t/d = 11$, the transition thickness is $H^* = 21.3d$. The change in regime, that is to say the transition, is assigned to the flow thickness H^*.

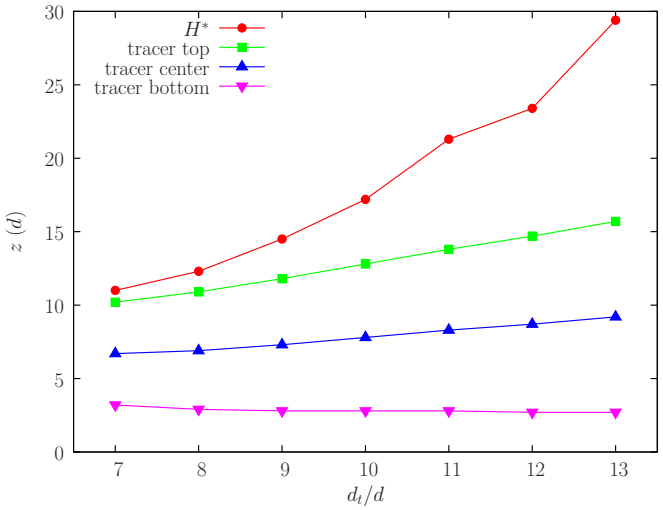

FIG. 14. Transition flow thickness H^* based on the tracer height difference, versus tracer size ratio d_t/d (red dots). The mean vertical locations of the tracer summit (green squares), center (blue triangles), and bottom (purple reverted triangle) for a flow of thickness H^* are also displayed.

Figure 14 summarizes the results for all size ratios. In addition to the transition flow thickness H^*, the mean vertical locations of the tracer summit and center for a flow of thickness H^* are also reported. These vertical locations have been obtained by interpolation of previous results since no flow with the exact flow thickness H^* have been simulated. As the tracer vertical location varies very weakly with the flow thickness (see inset of Fig. 11), the interpolation gives accurate results.

The comparison of the transition thickness H^* with the position of the tracer summit proves that the attractive/repulsive transition is not concomitant with the emergence of the tracers from the flow. Both tracers are fully embedded for a flow thickness H^*. Furthermore, Figure 14 shows that the transition thickness increases faster than the height of the tracers. The number of small flowing particles above the tracers at the transition is not constant with the size ratio d_t/d, nor proportional to d_t/d, but strongly increases, while the layer thickness of small particles between the tracer bottom and the rough incline slightly decreases.

Other criteria to define the transition thickness have been tested, like the intersection with any horizontal line, for example $\Delta z = 0.05d$, in Fig. 13. Figure 14 remains almost identical for all criteria and the conclusions are unchanged.

D. Slope of the incline

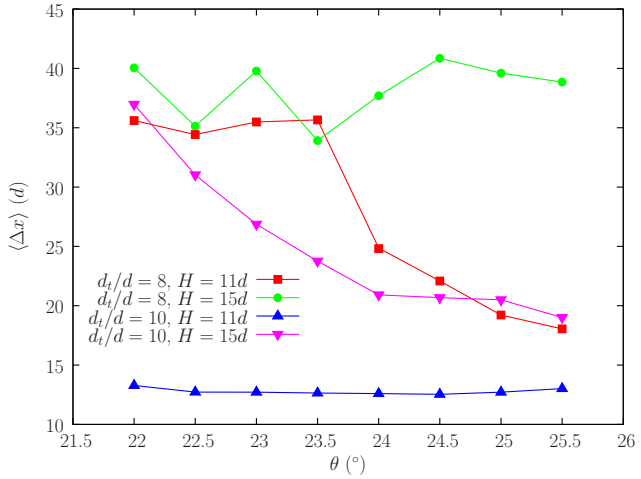

FIG. 15. Mean longitudinal distance $\langle \Delta x \rangle$ between two tracers versus slope: (red squares) $d_t/d = 8$ and $H = 11d$, (green circles) $d_t/d = 8$ and $H = 15d$, (blue triangles) $d_t/d = 10$ and $H = 11d$, and (purple reversed triangles) $d_t/d = 10$ and $H = 15d$.

The influence of the slope of the incline is now studied. Whereas previous results were all obtained for an angle of 24°, the incline angle θ is varied from 22° to 25.5° for four typical cases: an attractive case ($d_t/d = 10$, $H = 11d$) where tracers are almost in contact $\langle \Delta x \rangle \simeq d_t$, a repulsive case ($d_t/d = 8$, $H = 15d$) where tracers locate at their maximal distance $\langle \Delta x \rangle \simeq 40d$, and two intermediate situations ($d_t/d = 10$, $H = 15d$ and $d_t/d = 8$, $H = 11d$) where tracers are in an attractive regime, not

far from the attractive-repulsive transition, and locate at a intermediate distance.

Figure 15 reports the mean longitudinal distance between tracers, $\langle \Delta x \rangle$, versus slope angle for the four cases. For the two utmost cases, either attractive or repulsive, the variation in slope does not alter significantly the distance between tracers. For the two intermediate cases, increasing the slope angle favors the attractive regime and, conversely, decreasing the slope angle favors the repulsive regime. For the tracer diameter $d_t = 8d$, the transition is sharp and occurs between 23.5° and 24.5° while for the larger tracer diameter $d_t = 10d$, the transition is more progressive and occurs between 22° and 24°. This is reminiscent of the smoothing that is observed at increasing size ratio d_t/d for the transition in $\langle \Delta x \rangle$ with the flow thickness (see Fig. 10).

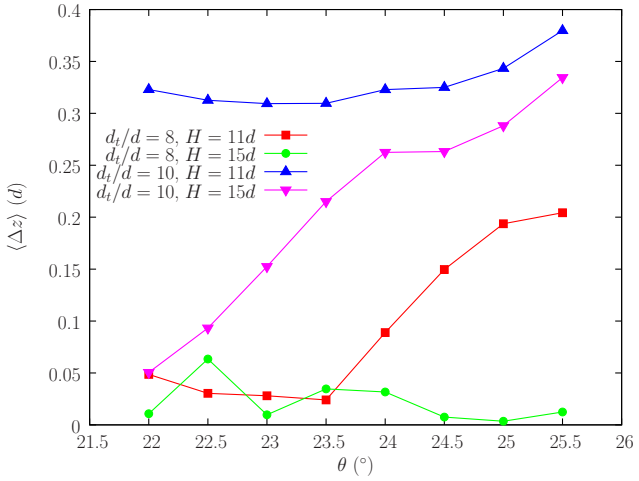

FIG. 16. Mean height difference $\langle \Delta z \rangle$ between two tracers versus slope: (red squares) $d_t/d = 8$ and $H = 11d$, (green circles) $d_t/d = 8$ and $H = 15d$, (blue triangles) $d_t/d = 10$ and $H = 11d$, and (purple reversed triangles) $d_t/d = 10$ and $H = 15d$.

Figure 16 reports the mean height difference between tracers, $\langle \Delta z \rangle$, versus slope angle, for the same four cases. Figure 16 is close to a vertical mirror of Fig. 15. When the system evolves toward the attractive regime for increasing slope angle, the longitudinal distance between tracers decreases and, simultaneously, the difference in height of the tracers increases.

On the whole, a variation in the angle of the incline has a rather weak impact on the attractive-repulsive transition and causes the tracers to switch from one regime to the other only when the system is already close to the transition. Nevertheless, increasing the slope favors the attracting regime, and as a consequence, increases the transition thickness H^*.

E. Incline roughness

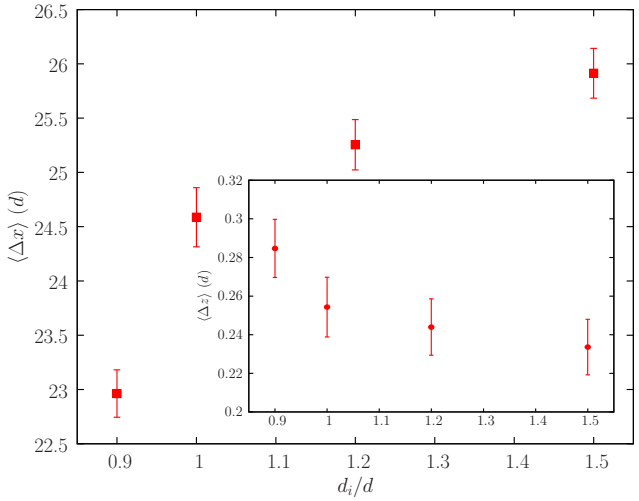

FIG. 17. Mean longitudinal distance between two tracers $\langle \Delta x \rangle$ versus incline roughness expressed by means of the size of the glued particles, from $0.9d$ to $1.5d$. (Inset) Corresponding mean height difference $\langle \Delta z \rangle$. The tracer size is $d_t/d = 10$, the flow thickness $H = 15d$ and the incline angle $\theta = 24°$. Error bars show a 95% interval of confidence of the mean value.

The roughness of the incline is now varied, for an incline angle of 24°, a size ratio $d_t/d = 10$ and a flow thickness $H = 15d$, one of the two previous intermediate case where tracers are in an attractive regime, not far from the attractive-repulsive transition, and locate at a defined distance. Up to now, the incline was made rough with glued particles of the same size, d, as the small flowing particles. Here, inclines with roughness created with glued particles of size $d_i = 0.9\,d$, d, $1.2\,d$ and $1.5\,d$ are investigated. An incline made rough with smaller particles, namely $d_i = 0.8\,d$, leads to a mean velocity of the flow which is extremely high, indicating that a slip occurs at the base of the flowing material. On the other hand, the roughness obtained with particles of size $d_i = 1.5\,d$ is known to generate the highest friction for a granular flow made of particle of size d [42] and the actual roughness of the incline is expected to decrease when larger particles are used because flowing particles fill the voids between them.

Figure 17 and its inset report the mean longitudinal distance, $\langle \Delta x \rangle$, and the mean height difference, $\langle \Delta z \rangle$, between the tracers for the four incline roughnesses, expressed by means of the size of the glued particles. A decrease in the size of the glued particles, i.e. a decrease in roughness, causes the system to evolve toward the attractive regime: the distance between tracers decreases and, simultaneously, the difference in height of the tracers increases. The variations in longitudinal distance $\langle \Delta x \rangle$ and height difference $\langle \Delta z \rangle$ between tracers with incline roughness being moderate, averaging over 500 s were necessary to obtain statistically significant mean values.

It can be noted that both increasing the incline angle and decreasing the incline roughness result in a shift to-

ward the attractive regime while implying an increase in the mean flow velocity. This can be used to compare the strength of these two effects. Simulations show that increasing the incline angle from 22° to 25.5° increases the mean flow velocity by a factor 4.3 and decreases the longitudinal distance between tracers by a factor $37/19 \simeq 1.9$. Likewise, decreasing the incline roughness from $d_i = 1.5\,d$ to $d_i = 0.9\,d$ increases the velocity by a factor 1.2 for a distance decrease by a factor $26.7/23.2 = 1.15$. Thus, in terms of variations of longitudinal distance versus flow velocity, the effect of incline roughness and incline angle are comparable.

V. A PROPOSED MECHANISM

All the above demonstrates a tight link between the horizontal and vertical positions of two large tracers interacting in a granular flow. More specifically, Fig. 15 and 16 show that a decrease in the mean longitudinal distance $\langle \Delta x \rangle$ between the tracers and an increase in their mean height difference $\langle \Delta z \rangle$ occur simultaneously when varying the incline angle. Figure 17 leads to the same evolution when modifying the incline roughness.

A variation in flow thickness yields a similar link between the longitudinal distance and the height difference, made a little more complex by the emergence of the tracers for thin flows. For flow thicknesses larger than the transition thickness H^*, tracers are far away from each other and locate at the same height. When the flow thickness is decreased below H^*, Fig. 10 and 13 show that the mean longitudinal distance $\langle \Delta x \rangle$ decreases and the mean height difference $\langle \Delta z \rangle$ increases simultaneously. This remains true until the tracers get close to the free surface. Below the flow thickness at which the tracers start to emerge from the granular flow, an extra buoyancy term due to the emerging part of the tracers counterbalances the interaction between tracers and reduces the height difference between them. This results in the non monotonous variation observed in Fig. 13: whereas the mean longitudinal distance $\langle \Delta x \rangle$ always decreases at decreasing flow thickness, the mean height difference $\langle \Delta z \rangle$ first increases, then decreases as the emerged part grows.

To figure out the mechanisms at play in the interaction between tracers, two additional numerical experiments were performed. The first simulation aims at analyzing the velocity of the granular flow in the neighborhood of the two tracers, the second simulation probes the reciprocal link that exists between the longitudinal and vertical distances between the tracers.

Figure 18 reports the velocity vector field and the tracer positions in the vertical reference frame (Oxz) of the front (right) tracer. Tracers have a diameter $d_t = 10d$ and are fully embedded in a granular flow of thickness $H = 15d$, smaller than the transition thickness H^* but larger than the flow thickness for which the tracers start to emerge. The slope is 24°. Because the relative tracer

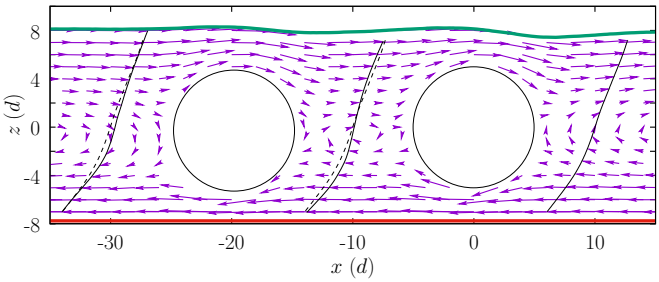

FIG. 18. Velocity map in the vertical plane in the reference frame (Oxy) of the front tracer (right tracer). The tracer size is $d_t/d = 10$, the flow thickness is $H = 15d$ and the slope is $\theta = 24°$. Tracers are at their relative equilibrium position: $\Delta x = 20d$ and $\Delta y = 0$. The thick green line stands for the free surface of the flow. The thick red line passes through the summit of the particles that are glued on the incline and form the incline roughness. Three continuous inclined black lines indicate the velocity profile measured in front of the tracers (right black line), between them (middle black line) and behind them (left black line). The two inclined dashed lines duplicate the front velocity profile, shifted horizontally to facilitate comparison.

positions Δx and Δy fluctuate with time, a specific procedure is necessary to reduce the amplitude of these fluctuations which would otherwise blur the measured velocity vector field around the tracers. This was achieved by adding two horizontal virtual springs between the tracers to force them to retain their relative position at equilibrium [12]. The fluctuations on the vertical distance being rather small, no spring was added in the z direction. From Fig. 8, the length of the spring aligned with the flow is $\Delta x_0 = 20d$ and the length of the transverse spring is $\Delta y_0 = 0$. The stiffness of the springs, k_x and k_y, are chosen to keep the fluctuations around the equilibrium relative position smaller than $0.5d$. After test and trial, a value of $k_x = k_y = k_n/20000$ is retained, where k_n is the stiffness of the normal repulsion spring between particles when in contact. The velocity field of Fig. 18 corresponds to the flow around two tracers being at their equilibrium relative position and is likely to differ from the real velocity field around tracers that move out of equilibrium due to fluctuations. This nevertheless helps to understand the involved mechanisms, as exposed below. Furthermore, it can be noted that the height difference Δz computed for the tracers joined by two horizontal springs convincingly agrees with that of free tracers (see Fig. 21).

When two particles are flowing, for instance spheres sedimenting in a liquid or cyclists, the back particle accelerates when in the drag of the front one. The picture is slightly more complex for tracers in a granular flow down an incline since they are in a shear flow. The tracers move faster than the small particles flowing below them and slower than the small particles flowing above them. In Fig. 18, the thin black line around $x = -10d$ delineates the velocity profile in between the two tracers

while the thin black lines around $x = 10d$ and $x = -30d$ delineate the velocity profile far ahead and far behind the tracers, respectively. To facilitate comparison, the velocity profile at $x = 10d$ has been duplicated in two dashed lines shifted around $x = -10d$ and $x = -30d$. This shows that, in the vertical direction and all over the height of the tracers, the velocity gradient is reduced between the tracers. In the lower part of the flow $-5d \lesssim z \lesssim -d$, the velocities of small particles are larger than far ahead of the tracers; the lower half of the back tracer is in the wake of the front tracer and the effect of this wake is to accelerate the back tracer until a new equilibrium position is reached. In the upper part of the flow $d \lesssim z \lesssim 5d$, the velocities of small particles are smaller than far away from the tracers; the upper half of the front tracer is in the wake of the back tracer and this decelerates the front tracer. In other words, each tracer is in the wake of the other (in its upper or lower half) and both wakes push the tracers to get closer. Since the closer the tracers are, the higher the wake effect is, the velocity gradient in the region between them further decreases and tracers should end up being in contact. However, an opposite mechanism causes the tracers to repel and derives from the height difference between the tracers. As they are embedded in a shear flow, the front tracer, which is higher, tends to go faster and the back tracer, which is lower, tends to go slower. As a consequence, the tracers tend to move away from each other. These two mechanisms counterbalance to place tracers at a defined equilibrium distance.

The origin of the height difference can also be apprehended from Fig. 18. All the small particles near the bottom of the flow move slower than the tracers. In addition, those that are jammed between the front tracer and the rough incline are subjected to a higher shear than those located further downstream. This makes the thin layer of small particles near the bottom easier to penetrate by the back tracer than by the front tracer, and lowers its equilibrium position in the flow. The closer the tracers are, the stronger this effect and the larger the height difference between them. The origin of the height difference can also be apprehended from Fig. 18. As discussed above, the wake effects experienced by the two tracers are not symmetrical as they operate on its lower part for the back tracer and on its upper part for the front tracer. This dissymmetry is expected to lead to different steady-state vertical positions for the tracers in the granular flow. Since both tracers necessarily flow at the same speed at equilibrium, the front tracer has to settle slighly upper and the back tracer slighly lower than their center of mass. The height difference between the tracers could also be enhanced by the alteration by the front tracer of the structure of the thin layer of small particles near the bottom. Because the small particles that are jammed between the front tracer and the rough incline are subjected to a higher shear than those located further downstream, the lowest layers of small particles are somewhat rearranged and eventually easier to penetrate by the back tracer. This contributes to lower its equilibrium position in the flow. The closer the tracers are, the stronger these effects and the larger the height difference between them.

The emergence of the tracers makes the picture a little more complex. Figure 19 is the counterpart of Fig. 18 for a flow thickness $H = 9d$. The length of the longitudinal spring equals the equilibrium longitudinal distance between the tracers and is thus reduced to $\Delta x_0 = 12.5d$. Other parameters are unchanged. Figure 19 shows that the shear between the tracers is reduced compared to the case $H = 15d$. As shown previously, the thinner the flow, the more the tracers emerge and the more the height difference between them is reduced by the additional buoyancy term. This weakens the repulsive effect provided by the height difference. Furthermore, there is no more small particles flowing at the summit of the tracers also reducing the repulsive effect. The attractive effect due to the wake is likely to reduce too since the overall velocities are reduced in a flow with a lower thickness, but as tracers are closer compared to the thick flow case, the repulsive effect is more affected than the attraction.
As shown previously, the thinner the flow, the more the tracers emerge and the more the height difference between them is reduced by the additional buoyancy term. The repulsive effect due to the height difference reduces in turn. Furthermore, there is no longer small particles flowing near the top of the tracers, which further reduces the repulsive effect. The attractive effect due to the wake is likely to weaken too since velocities are overall smaller in a flow with a lower thickness, but the repulsive effect is expected to be more affected than the attraction since tracers end up closer.

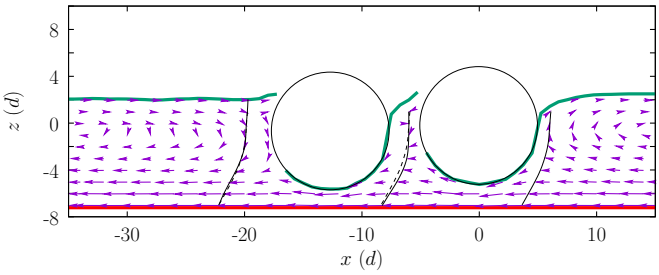

FIG. 19. Same as Fig. 18 except that the flow thickness is $H = 9d$. Tracers are at their relative equilibrium position: $\Delta x = 12.5d$ and $\Delta y = 0$. Tracers emerge from the free surface of the flow (thick green line).

To further explore the link between the longitudinal distance and the height difference between the tracers, and hence the mechanisms involved in the convergence of the tracers, another numerical experiment is performed with only one vertical (perpendicular to the incline) virtual spring. The spring length is null $\Delta z_0 = 0$ and its stiffness is increased from $k_z = 0$ to $k_z = k_n/100$ to probe an increasingly strong constraint on the height difference of the tracers in the flow and to decrease the repulsive effect between tracers. As there is no longer horizontal

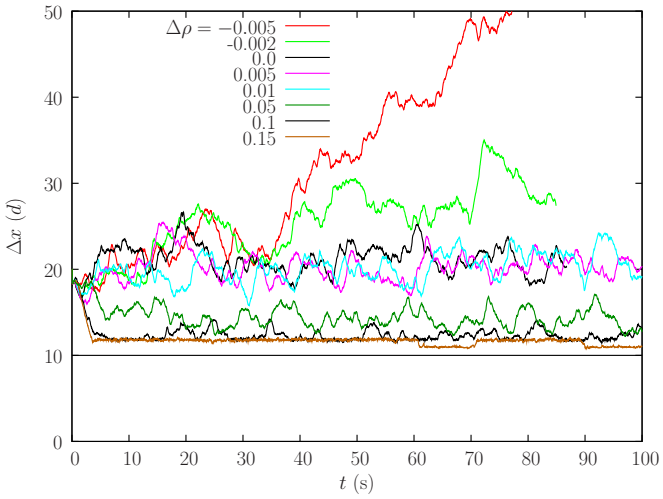

FIG. 20. Time evolution of the longitudinal distance Δx between two tracers having a density difference. The tracer size is $d_t/d = 10$, the flow thickness is $H = 15d$ and the slope is $\theta = 24°$. The density perturbation varies from $\Delta\rho = -0.005$ (front tracer is lighter) to $\Delta\rho = 0.15$ (front tracer is heavier).

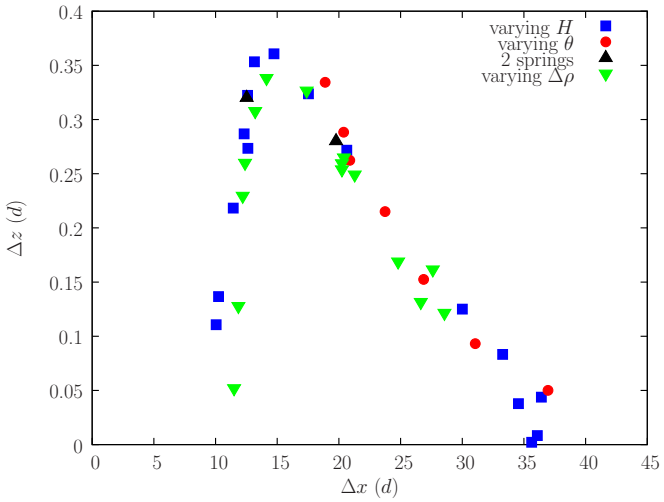

FIG. 21. Height difference Δz versus longitudinal distance Δx between tracers at equilibrium for various density perturbation (green inverted triangle). The size ratio is $d_t/d = 10$, the flow thickness $H = 15\,d$ and the slope $\theta = 24°$. The link between Δz and Δx is also extracted by varying the flow thickness H (blue square) for a slope of 24°, and by varying the slope (red circles) for a flow thickness $H = 15\,d$, both without density difference. The case of tracers linked by two horizontal springs is also reported (Figs. 18 and 19) for $H = 15\,d$ and $9\,d$, and for a slope of 24° (black triangle).

(parallel to the incline) springs to constrain them, the longitudinal and transverse distances between the tracers are expected to relax to equilibrium values that differ from those obtained without the vertical spring. Their dependency on the height difference Δz is studied.

To further explore the link between the longitudinal distance and the height difference between the tracers, and hence the mechanisms involved in the convergence of the tracers, another numerical experiment is performed where the density of the tracers are slightly modified to increase or decrease the height difference Δz. The density of the front tracer is multiplied by $1 + \Delta\rho$ where $\Delta\rho$ may be positive or negative. Symmetrically, the density of the back tracer is multiplied by $1 - \Delta\rho$.

The configuration of two tracers fully embedded in the granular flow is considered again, with a tracer diameter $d_t = 10d$, a flow thickness $H = 15d$, and a slope of 24°. Tracers are initially aligned $\Delta y = 0$ and located at a longitudinal distance $\Delta x = 20d$ close to their equilibrium distance at this flow thickness. Figure 20 shows the time evolution of Δx for the various density difference $\Delta\rho$. The larger the density difference is, the closer the tracers, showing a reduction of the repulsion effect.

Figure 21 reports all the numerical results on the longitudinal and vertical distances between tracers of diameter $d_t = 10d$ obtained by changing the density of the two tracers. Each couple $(\Delta x, \Delta z)$ has been obtained by averaging over a period of 50 s, the first 50 s of the simulation being discarded to ensure convergence. The previous results obtained by varying the thickness of the flow H for a slope of 24° (large blue squares) and by varying the slope angle for a flow thickness $H = 15d$ (large red dots) are also reported in Fig. 21, as well as the two points from the simulations with two horizontal springs (large black triangle).

The most remarkable fact here is that the series corresponding to the various density perturbation are organised to follow the overall curve evolution given by the variation of H and θ. This suggests that the height difference Δz, obtained either naturally by changing the slope or the flow thickness, or reduced somehow artificially by changing the density of the tracers, imposes the longitudinal equilibrium distance Δx between the flowing tracers.

Note that the two points (large black triangle) showing the couples $(\Delta x, \Delta z)$ obtained when two horizontal springs were used to compute the velocity maps of Figs. 18 and 19 perfectly match with the others. This confirms that the horizontal springs are weak enough not to perturb the relative tracer position compared to the case of free tracers, as stated in the description of the precedure used to evaluate the velocity maps.

The left, decreasing side of Fig. 21 shows that the reduction of the height difference between tracers Δz, either because the flow is thin and tracers emerge, or because a larger density difference forces Δz to decrease, causes the longitudinal distance between tracers Δx to also decrease. In contrast, when the flow thickness increases, the shear of the granular flow and thus the repulsive effect increases while the tracers benefit less and less from the wake of the other tracer. As a consequence, they move apart from each other and eventually do not interact at all. This confirms that the mechanism that moves away tracers is their height difference in a flow

with a vertical shear.

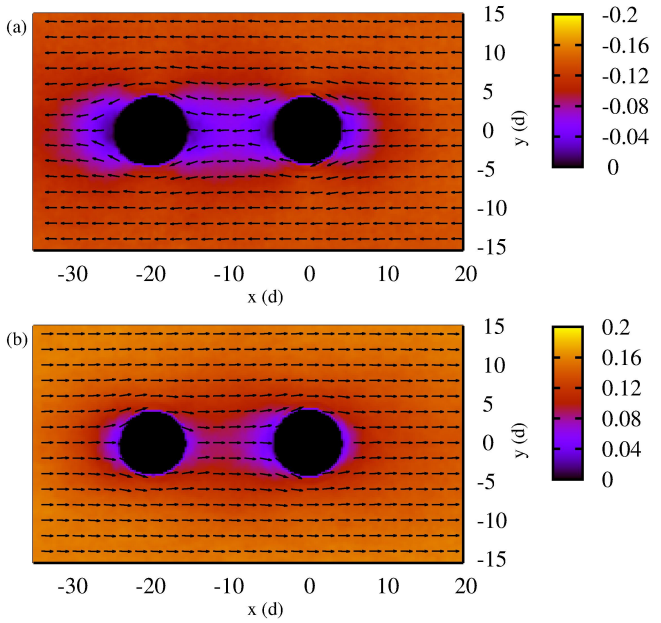

FIG. 22. Velocity map in the horizontal plane Oxy at a distance of $2.5d$ below (a) and above (b) the center of the front tracer in the reference frame of this tracer (right tracer). The tracer size is $d_t/d = 10$, the flow thickness is $H = 15d$ and the slope is 24°. All vectors have the same length and the color map indicates the velocity in m/s.

Another question that remains to be answered is why tracers align with the flow. Figure 22 shows two velocity maps in planes parallel to the incline and located half way between the center and the bottom of the front tracer (Fig. 22(a)) and half way between the center and the top of the front tracer (Fig. 22(b)), which corresponds to $z = -2.5\,d$ and $z = 2.5\,d$ in Fig. 18, respectively. The reference frame is that of the front tracer. The darker zones between the tracers show the wake made by the front tracer in Fig. 22(a) and the wake made by the back tracer in Fig. 22(b). Note that Fig. 22 remarkably illustrates the difference in the wake effects felt by the tracers due to the velocity gradient that characterizes a shear flow. As soon as the back tracer is out of alignment, it is pushed back to the in-line position by the small particles that flow at the side of the tracers and that move faster than the small particles in the wake region of the front tracer (see the color code of Fig. 22(a)). The counterpart situation is observed in the upper plane $z = 2.5d$ where the front tracer is in the wake of the back tracer (Fig. 22(b)). In the attracting regime, tracers are close, the wake is strong and tracers are perfectly aligned. In the repelling regime, tracers are distant, they weakly feel the wake of the other tracer and the transverse distance strongly fluctuates.

VI. CONCLUSION

The interaction of two large tracers in a flow down a rough incline depends on flow thickness, roughness of the incline, slope and size of the tracers. Tracers always align because tracers are embedded in a shear flow and depending on the height, each tracer is in the wake of the other tracer. This effect align them and also tends to get them close from each other. In addition, tracers are floating just above the bottom, at an equilibrium level inside the flow. This equilibrium results from their high density compare to the bulk density of the small particles plus the void between them, and the difficulty for a tracer to penetrate very close to the rough incline because of efficient chain forces in the first 2-3 layers of small particles. These large tracers are in a reverse segregated position. The chain forces through small particles near the bottom slow down the tracer. Nevertheless, it is possible for a tracer to get further close to the incline, either if the structure of the flow is modified, either by increasing the force (increasing tracer density for example) endured by the tracer to get down. When the back tracer is in the path of the front one, the back tracer experiences a modified structure of the flow and it gets closer to the bottom than the front tracer. In addition, the two tracers go faster than a unique tracer, and this lift the front tracer. The resulting height difference between tracers is very small, but enough to ensure that both tracers are surrounded by small particles with a slightly different velocity. The center of mass of the front tracer being upper in the velocity gradient of the flow, it tends to move faster than if it was in a lower position. The height difference between tracers in a velocity gradient tends to repel the two tracers. The resulting relative positions of the two tracers comes from the balance between the wake effect and the height difference. The interaction between two tracers implies equilibrium position of reverse segregation in accordance with their velocity and the flow structure, and velocity gradient of the flow that depends on the flow thickness, slope and roughness of the incline.

This explains why the increase of flow thickness, the decrease of slope, the increase of roughness, the decrease of tracer size all tend to repel the tracers.

This paper reports experiments and DEM simulations on the interaction of two large particles in a flow of small particles down a rough incline. All particles have the same density and the size ratios between the large and the small particles are chosen to lead to reverse segregation. It is shown that the two large particles, called tracers, do interact. They are seen to systematically align in the direction of the flow while their longitudinal arrangement varies from tracers in contact to tracers far away from each other, according to various parameters. Thus, when the thickness of the flow increases, all else being equal, the interaction between the tracers changes from an attractive to a repulsive regime. A tendency for the front tracer to rise and for the back tracer to sink is also observed. The resulting difference in height of the tracers

within the flow conveniently provides a criterion on the flow thickness for the transition between the attractive and repulsive regimes.

The effects of the size of the tracers as well as the slope and the roughness of the incline on the interaction between the two tracers have been investigated. The thorough parametric study performed reveals a tight link between the equilibrium longitudinal distance between the tracers and their height difference in the flow.

Numerical simulations make it possible to properly capture the flow in the vicinity of the tracers and the velocity field around the tracers gives clues about the interaction mechanism. Because of the wake effect of each tracer on the other and because tracers are embedded in a shear flow, they are pushed back in line with each other and tend to get closer. Simultaneously, still due to the velocity gradient in a shear flow, the difference in height between the tracers, however small, tends to drive the tracers away since the back tracer, lower, goes slower than the front tracer, upper in the flow. A finite equilibrium separation stems from the balance between these two effects, wake and height difference, and the two large particles are found to attract or repel each other depending on the flow conditions. As for the height difference between the tracers, with the front tracer higher than the back tracer, it primarily originates from the dissymmetry induced by the shear flow on the wake effect exerted by each of the two tracers, although other mechanisms may be involved. As a matter of fact, the size ratios between the tracers and the small particles that have been implemented are such that the tracers are in a reverse segregated position, close to the bottom of the flow. The first two to three layers of small particles above the incline are very hard to penetrate, but the back tracer experiences a structure of the flow in these lowermost layers which has been modified by the front tracer and this may bring it closer to the bottom. More generally, the equilibrium heights of the tracers result from their velocities and the flow structure. The underlying microstructure dynamics needs to be further investigated and its subtle role in the physical mechanisms of the interaction between two large particles in a granular shear flow will be the focus of future work. Nevertheless, the analysis already performed in the present study provides insight into the dependence of the interaction process on the flow thickness and on the slope and roughness of the incline.

The interaction between large particles can be of major interest in natural flows or industrial problems. Internal organizations distinct from the size segregation induced patterns may be expected, such as the formation of trains of tracers. Consequences of these new organizations, especially on the rheology of granular flows, deserve to be investigated.

In many respects, the behaviors reported in this article are reminiscent of those exhibited by pairs of particles settling in fluids. It would be interesting to explore the similarities and differences in the underlying mechanisms.

ACKNOWLEDGMENTS

Centre de Calcul Intensif d'Aix-Marseille University is acknowledged for granting access to its high performance computing resources.

[1] K. K. Rao, P. R. Nott, and S. Sundaresan, *An introduction to granular flow* (Vol. 490), Cambridge University Press (2008).
[2] J. Duran, *Sands, powders, and grains: an introduction to the physics of granular materials*, Springer Science & Business Media (2012).
[3] B. Andreotti, Y. Forterre, and O. Pouliquen, *Granular media: between fluid and solid*, Cambridge University Press (2013).
[4] J. M. Ottino and D. V. Khakhar, Mixing and segregation of granular materials, Annu. Rev. Fluid Mech. **32**, 55 (2000).
[5] E. Clement, J. Rajchenbach, and J. Duran, Europhys. Lett. **30**, 7 (1995).
[6] F. Cantelaube and D. Bideau, Europhys. Lett. **30**, 133 (1995).
[7] N. Thomas, Phys. Rev. E **62**, 961 (2000).
[8] G. Félix and N. Thomas, Phys. Rev. E **70**, 051307 (2004).
[9] N. Thomas and U. D'Ortona, Phys. Rev. E **97**, 022903 (2018).
[10] R. López de la Cruz and G. Caballero-Robledo, J. Fluid Mech. **800**, 248 (2016).
[11] G. A. Caballero-Robledo, M. F. Acevedo-Escalante, F. Mandujano, and C. Má laga Phys. Rev. Fluids **6**, 084303 (2021).
[12] F. Guillard, Y. Forterre, and O. Pouliquen, J. Fluid Mech. **807** (2016).
[13] M. Smoluchowski, Bull. Acad. Sci. Cracow **1A**, 28 (1911).
[14] M. Mason and W. Weaver, Phys. Rev. **23**, 412 (1924).
[15] G. J. Kynch, Trans. Faraday Soc. **48**, 166 (1952).
[16] J. F. Richardson and W. Zaki, Trans. Inst. Chem. Eng. **32**, 35 (1954).
[17] J. Happel and H. Brenner, *Low Reynolds Number Hydrodynamics*, Prentice-Hall (1965).
[18] G. K. Batchelor, J. Fluid Mech. **52** 245 (1972).
[19] G. K. Batchelor, J. Fluid Mech. **119** 379 (1982).
[20] L. Durlofsky, J. F. Brady, and G. Bossis, J. Fluid Mech. **180**, 21 (1987).
[21] S. Kim and S. J. Karrila, *Microhydrodynamics: Principles and Selected Applications*, Butterworth-Heinemann, (2005).
[22] A. Doostmohammadi and A. M. Ardekani, Phys. Rev. E **88**, 023029 (2013).
[23] A. Fortes, D. Joseph, and T. Lundgren, J. Fluid Mech. **177**, 467 (1987).
[24] R. Sun and A. Chwang, Phys. Rev. E **76**, 046316 (2007).
[25] J. Favier, A. Revell, and A. Pinelli, J. Comp. Phys. **261**, 145 (2014)

[26] K. O. L. F. Jayaweera and B. J. Mason, Experiment. J. Fluid Mech. **20**, 121 (1963).
[27] B. Metzger , M. Nicolas and E. Guazelli, J. Fluid Mech. **580**, 283 (2007).
[28] A. El Yacoubi, S. Xu, and Z. J. Wang, J. Fluid Mech. **705**, 134 (2012)
[29] J.-P. Matas, V. Glezer, E. Guazzelli, and J. F. Morris, Phys. Fluids **16**, 4192 (2004)
[30] K. J. Humphry, P. M. Kulkarni, D. A. Weitz, J. F. Morris, and H. A. Stone, Phys. Fluids **22**, 081703 (2010)
[31] I. S. Santos de Oliveira, A. van den Noort, J. T. Padding, W. K. den Otter, and W. J. Briels, J. Chem. Phys. **135**, 104902 (2011)
[32] P. A. Cundall and O. D. L. Starck, Géotechnique **29**, 47 (1979).
[33] J. Schäfer, S. Dippel, and D. E. Wolf, J. Phys. 1 (France) **6**, 5 (1996).
[34] U. D'Ortona, N. Thomas, and R. M. Lueptow, Rev. E **93**, 022906 (2016).
[35] Z. Zaman, U. D'Ortona, P. B. Umbanhowar, J. M. Ottino, and R. M. Lueptow, Phys. Rev. E **88**, 012208 (2013).
[36] N. Taberlet, M. Newey, P. Richard, and W. Losert, J. Stat. Mech. P07013 (2006).
[37] P. Chen, J. M. Ottino, and R. M. Lueptow, New J. Phys. **13**, 055021 (2011).
[38] G. H. Ristow, Pattern Formation in Granular Materials (Springer-Verlag, Berlin, 2000).
[39] See Supplemental Material at [href will be inserted by editor].
[40] C. S. Campbell, J. Fluid Mech. **465**, 261 (2002).
[41] L. E. Silbert, G. S. Grest, R. Brewster, and A. J. Levine, Phys. Rev. Lett. **99**, 068002 (2007).
[42] C. Goujon, N. Thomas, and B. Dalloz-Dubrujeaud, Euro. Phys. J. E **11**, 147 (2003).